ISSN 1995-4239, Numerical Analysis and Applications, 2020, Vol. 13, No. 3, pp. 271–281. © Pleiades Publishing, Ltd., 2020.
Russian Text © The Author(s), 2020, published in Sibirskii Zhurnal Vychislitel'noi Matematiki, 2020, Vol. 23, No. 3, pp. 325–338.

Numerical Modeling with a Grid-Characteristic Method of Elastic Wave Propagation in Geological Media with Gas Cavities

P. V. Stognii[1*], N. I. Khokhlov[2], and I. B. Petrov[1,2***]**

[1] *Moscow Institute of Physics and Technology, Institutskii per. 9, Dolgoprudnyi, Moscow Region, 141700 Russia*

[2] *Scientific Research Institute for System Analysis, Russian Academy of Sciences, Nakhimovskii pr. 36/1, Moscow, 117218 Russia*

Received April 11, 2019; in final form, June 12, 2019; accepted April 16, 2020

Abstract—Shallow gas in ground water geological layers is of great danger for drilling rigs in the case of accidental opening of gas deposits. The gas may rise towards the water surface, and its emission into the atmosphere may threaten the environment. It is very important to forecast the gas emissions in order to prevent catastrophic destruction of drilling rigs and loss of human lives. This paper presents the results of numerical simulations of seismic wave propagation towards the water surface in models with gas deposits in a layered soil for the 3D case. The modeling is carried out for a 4-year period for layers located at a depth of 1000 m from the sea bottom. The calculation results (wave patterns and seismograms) show that the gas may approach the water surface in the 4th year of the calculations. The results for a 3D problem are in agreement with those for a 2D problem obtained by the authors earlier. This is very important, since the calculations can be greatly simplified.

DOI: 10.1134/S1995423920030076

Keywords: *gas pockets, numerical 3D modelling, grid-characteristic method, Arctic shelf.*

1. INTRODUCTION

Gas pockets or near-surface gas are gas reservoirs with anomalously high reservoir pressure (AHRP) [1–4]. Such gas reservoirs can be located at small (30–100 m) and considerable (1000 m) depths from the sea bottom. To date these gas pockets have been considered not dangerous, since spontaneous emissions have been very rare. However, arbitrary gas emissions into the atmosphere become more frequent due to global warming. This is because many gas pockets hidden in frozen rocks are no longer gas-tight and begin to spread to the water surface. There are also gas emissions into the atmosphere due to earthquakes [5].

Accidental opening of gas reservoirs by drilling rigs often takes place. Due to high pressure in the reservoirs, the gas rises to the surface and enters the atmosphere. This may cause loss of human lives, damage to the rigs, and increase the gas content in the water. A severe accident took place in the Gulf of Mexico in 2010 largely as a result of a gas emission with AHRP. it killed 11 people, destroyed a modern drilling rig, and caused the penetration of a large amount of oil into the gulf (about 0.7 million tons). To avoid serious consequences from such emissions and undertake timely measures, systematic monitoring of the territories with gas deposits is required.

Gas pockets are widespread in the North Seas. For instance, the number of only known gas deposits in the Sea of Okhotsk is about 200 [6], and on the Netherlands shelf it is 150 [7]. Gas pockets can also be found in the Barents, Pechora, and Kara Seas [8]. Monitoring of all such gas deposits becomes more difficult every year due to their rapid increase in number and high cost of geological exploration. To avoid

[*] E-mail: stognii@phystech.edu
[**] E-mail: k_h@inbox.ru
[***] E-mail: petrov@mipt.ru

frequent monitoring of territories with gas pockets, it is proposed to simulate the development of the detected gas deposits to undertake timely measures aimed at preventing the catastrophic consequences of possible gas emissions into the atmosphere.

This paper presents the results of three-dimensional simulations of the propagation of seismic waves in models with gas pockets in a layered structure towards the water surface. Such modeling has already been carried out for the two-dimensional case and, since the results turned out to be rather realistic (see [9, 10]), a similar study is performed for the three-dimensional case aimed at obtaining more complete information about wave processes in media with gas reservoirs. The thus obtained wave patterns of responses [11] of gas-saturated media for the 2nd, 3rd, and 4th years of calculations have shown that the gas pockets can approach the water surface on the 4th year of calculations. Seismograms of the 2nd, 3rd, and 4th years of calculations (except for those of the 1st year of calculations, in which no gas pockets were assumed to be present) have also shown an approach of the gas to the water surface in the 4th year of calculations. The results of the three-dimensional simulations turned out to be similar to those of a two-dimensional simulation of seismic wave propagation in models with gas saturated rocks during a period of four years. This will make it possible to replace the three-dimensional model with a two-dimensional one to simplify and speed up the calculations.

2. MATHEMATICAL MODEL

To describe various dynamic processes in heterogeneous geological media, the following system of equations for a linear elastic medium is used [12]:

$$\rho\frac{\partial \boldsymbol{v}}{\partial t} = \nabla\cdot\boldsymbol{\sigma}^{\top}, \tag{1}$$

$$\frac{\partial}{\partial t}\,\sigma = \lambda(\nabla\cdot\boldsymbol{v})I + \mu\big(\nabla\otimes\boldsymbol{v} + (\nabla\otimes\boldsymbol{v})^{\top}\big), \tag{2}$$

where ρ is the density of the material, v is the velocity, σ is the Cauchy stress tensor, λ and μ are the Lame parameters determining the properties of the elastic material, I is the unit tensor, and p is the pressure. In this study the water medium is also described by equations of linear elasticity (1), (2) with a transverse sound speed close to zero.

3. NUMERICAL METHOD

In this paper, a grid-characteristic method [13, 14] is used to numerically solve the system of equations (1), (2). This method allows constructing correct numerical algorithms to calculate points on the boundaries and points lying on the interfaces between two media with different densities and different Lame parameters. Let us present the system of equations (1), (2) in the following form:

$$\rho\frac{\partial}{\partial t}\boldsymbol{v}_j = \frac{\partial\sigma_{ji}}{\partial x_i}, \tag{3}$$

$$\frac{\partial}{\partial t}\,\sigma_{ij} = \lambda\left(\sum_k \frac{\partial v_k}{\partial x_k}\right)I_{ij} + \mu\big(\nabla_i v_j + \nabla_j v_i\big), \tag{4}$$

and rewrite the system of equations (3), (4) in matrix form as follows:

$$\frac{\partial \boldsymbol{q}}{\partial t} + \boldsymbol{A}_1\frac{\partial \boldsymbol{q}}{\partial x_1} + \boldsymbol{A}_2\frac{\partial \boldsymbol{q}}{\partial x_2} + \boldsymbol{A}_3\frac{\partial \boldsymbol{q}}{\partial x_3} = 0, \tag{5}$$

where $\boldsymbol{q}$ is a vector consisting of three components of velocity and six components of the symmetric stress tensor:

$$\boldsymbol{q} = \{\upsilon_x, \upsilon_y, \upsilon_z, \sigma_{xx}, \sigma_{yy}, \sigma_{zz}, \sigma_{xy}, \sigma_{xz}, \sigma_{yz}\}^\top. \tag{6}$$

In (5), $\boldsymbol{A}_1$, $\boldsymbol{A}_2$, and $\boldsymbol{A}_3$ are matrices which have the following form:

$$\boldsymbol{A}_1 = \begin{pmatrix} 0 & 0 & 0 & -1/\rho & 0 & 0 & 0 & 0 & 0 \\ 0 & 0 & 0 & -1/\rho & 0 & 0 & 0 & 0 & 0 \\ 0 & 0 & 0 & 0 & 0 & 0 & 0 & -1/\rho & 0 \\ -\lambda-2\mu & 0 & 0 & 0 & 0 & 0 & 0 & 0 & 0 \\ 0 & -\lambda & 0 & 0 & 0 & 0 & 0 & 0 & 0 \\ 0 & 0 & -\lambda & 0 & 0 & 0 & 0 & 0 & 0 \\ 0 & -\mu & 0 & 0 & 0 & 0 & 0 & 0 & 0 \\ 0 & 0 & -\mu & 0 & 0 & 0 & 0 & 0 & 0 \\ 0 & 0 & 0 & 0 & 0 & 0 & 0 & 0 & 0 \end{pmatrix}, \tag{7}$$

$$\boldsymbol{A}_2 = \begin{pmatrix} 0 & 0 & 0 & 0 & 0 & 0 & -1/\rho & 0 & 0 \\ 0 & 0 & 0 & 0 & -1/\rho & 0 & 0 & 0 & 0 \\ 0 & 0 & 0 & 0 & 0 & 0 & 0 & 0 & -1/\rho \\ 0 & -\lambda & 0 & 0 & 0 & 0 & 0 & 0 & 0 \\ 0 & -\lambda-2\mu & 0 & 0 & 0 & 0 & 0 & 0 & 0 \\ 0 & -\lambda & 0 & 0 & 0 & 0 & 0 & 0 & 0 \\ -\mu & 0 & 0 & 0 & 0 & 0 & 0 & 0 & 0 \\ 0 & 0 & 0 & 0 & 0 & 0 & 0 & 0 & 0 \\ 0 & 0 & -\mu & 0 & 0 & 0 & 0 & 0 & 0 \end{pmatrix}, \tag{8}$$

$$\boldsymbol{A}_3 = \begin{pmatrix} 0 & 0 & 0 & 0 & 0 & 0 & 0 & -1/\rho & 0 \\ 0 & 0 & 0 & 0 & 0 & 0 & 0 & 0 & -1/\rho \\ 0 & 0 & 0 & 0 & 0 & -1/\rho & 0 & 0 & 0 \\ 0 & 0 & -\lambda & 0 & 0 & 0 & 0 & 0 & 0 \\ 0 & 0 & -\lambda & 0 & 0 & 0 & 0 & 0 & 0 \\ 0 & 0 & -\lambda-2\mu & 0 & 0 & 0 & 0 & 0 & 0 \\ 0 & 0 & 0 & 0 & 0 & 0 & 0 & 0 & 0 \\ -\mu & 0 & 0 & 0 & 0 & 0 & 0 & 0 & 0 \\ 0 & -\mu & 0 & 0 & 0 & 0 & 0 & 0 & 0 \end{pmatrix}. \tag{9}$$

Applying a method based on splitting of the spatial dimensions to equation (5), we obtain three systems of one-dimensional equations [15]:

$$\frac{\partial \boldsymbol{q}}{\partial t} = \boldsymbol{A}_j \frac{\partial \boldsymbol{q}}{\partial x_j}, \quad j = 1, 2, 3. \tag{10}$$

Each of the systems (10) is hyperbolic and has a full set of eigenvectors with real eigenvalues. Therefore, each of the systems (10) can be presented as

$$\frac{\partial \boldsymbol{q}}{\partial t} = {\boldsymbol{\Omega}_j}^{-1} \boldsymbol{\Lambda}_j \boldsymbol{\Omega}_j \frac{\partial \boldsymbol{q}}{\partial x_j}, \tag{11}$$

where $\boldsymbol{\Omega}_j$ is a matrix consisting of the eigenvectors, and $\boldsymbol{\Lambda}_j$ is a diagonal matrix with the eigenvalues on the diagonal. In what follows the subscript j will be omitted for simplicity, and the case of only one of the space coordinates will be considered.

For all coordinates, the matrix $\boldsymbol{\Lambda}$ is

$$\boldsymbol{\Lambda} = \mathrm{diag}\{c_1, -c_1, c_2, -c_2, c_2, -c_2, 0, 0, 0\}, \tag{12}$$

where $c_1 = \sqrt{(\lambda + 2\mu)/\rho}$ is the longitudinal speed of sound, and $c_2 = \sqrt{\mu/\rho}$ is the transverse speed of sound.

Carrying out the change of variables $\boldsymbol{\nu} = \boldsymbol{\Omega q}$, we split each of the systems (11) into nine independent scalar advection equations:

$$\frac{\partial \boldsymbol{\nu}}{\partial t} + \boldsymbol{\Lambda} \frac{\partial \boldsymbol{\nu}}{\partial x} = 0. \tag{13}$$

The one-dimensional advection equations can be solved by a method of characteristics or using a finite-difference scheme. Once all components $\boldsymbol{\nu}$ are calculated, we can find the solution

$$\boldsymbol{q}^{n+1} = \boldsymbol{\Omega}^{-1} \boldsymbol{\nu}^{n+1}. \tag{14}$$

To solve the advection equations (13), we used a grid-characteristic method based on the third order accurate Rusanov scheme (see [16, 17]):

$$\nu_m^{n+1} = \alpha_{-2} \nu_{m-2}^n + \alpha_{-1} \nu_{m-1}^n + \alpha_0 \nu_m^n + \alpha_1 \nu_{m+1}^n, \tag{15}$$

where α_{-2}, α_{-1}, α_0, and α_1 are coefficients that can be found from the condition of third-order approximation for the scheme by expanding it in a Taylor series about, for instance, the point $({x_m}^n)$. The conditions for the second, third, etc. order approximation are determined from the relation

$$-(-\sigma)^k + \sum_{\mu,\nu} (\mu - \nu\sigma)^k {\alpha_\mu}^\nu(\sigma) = 0, \tag{16}$$

where $k = 2, 3, \ldots$; $\mu = 0, \pm 1, \ldots$; $\nu = 1, 0, -1, \ldots$; $\sigma = \frac{\boldsymbol{\Lambda}\tau}{h}$, λ is the speed of advection, τ is the step of integration in time, and h is the step of integration in the coordinate.

Our scheme is third order approximate. Hence, we obtain four equations of the form (16) for $k = 0, 1, 2, 3$ for finding the coefficients α_{-2}, α_{-1}, α_0, α_1:

$$\alpha_{-2} + \alpha_{-1} + \alpha_0 + \alpha_1 = 1, \tag{17}$$

$$-2\alpha_{-2} - \alpha_{-1} + \alpha_1 = -\sigma, \tag{18}$$

$$4\alpha_{-2} + \alpha_{-1} + \alpha_1 = \sigma^2, \tag{19}$$

$$-8\alpha_{-2} - \alpha_{-1} + \alpha_1 = -\sigma^3. \tag{20}$$

To regularize the numerical solution, a monotonicity criterion [16] was used, which has the following form for positive values of $\lambda > 0$:

$$\min\{\nu_m^n, \nu_{m-1}^n\} \leqslant \nu_m^{n+1} \leqslant \max\{\nu_m^n, \nu_{m-1}^n\}, \tag{21}$$

and for negative values of $\lambda < 0$ this criterion is symmetric.

4. BOUNDARY CONDITIONS

To calculate the points on the boundaries of the integration domain, the following equation is used [18]:

$$\boldsymbol{B}\boldsymbol{q}^{n+1} = \boldsymbol{b}, \tag{22}$$

where $\boldsymbol{B}$ is a 3×9 matrix, $\boldsymbol{b}$ is a three-dimensional vector, and $\boldsymbol{q}^{n+1}$ is the vector of velocity and stress tensor components at a point on the integration domain boundary at the next time level, $n+1$.

The solution (14) at the next time level, $n+1$, is as follows:

$$\boldsymbol{q}^{n+1} = \boldsymbol{\Omega}^{(\text{in})}\boldsymbol{\nu}^{n+1(\text{in})} + \boldsymbol{\Omega}^{(\text{out})}\boldsymbol{\nu}^{n+1(\text{out})} = \boldsymbol{q}^{n+1(\text{in})} + \boldsymbol{\Omega}^{(\text{out})}\boldsymbol{\nu}^{n+1(\text{out})}, \tag{23}$$

where $\Omega^{(\text{in})}$ and $\Omega^{(\text{out})}$ are matrices consisting of columns corresponding to the incoming and outgoing characteristics of the matrix Ω^{-1}; $\nu^{n+1(\text{in})}$ can be calculated in the same way as ν^{n+1} for internal points; $\nu^{n+1(\text{out})}$ is found from the boundary conditions (22):

$$\nu^{n+1(\text{out})} = \left(\boldsymbol{B}\boldsymbol{\Omega}^{(\text{out})}\right)^{-1}\left(\boldsymbol{b} - \boldsymbol{B}\boldsymbol{q}^{n+1(\text{in})}\right). \tag{24}$$

Substituting (24) into (23), we obtain a general formula for calculating the points on the integration domain boundaries:

$$\boldsymbol{q}^{n+1} = \boldsymbol{q}^{n+1(\text{in})} + \boldsymbol{\Omega}^{(\text{out})}\left(\boldsymbol{B}\boldsymbol{\Omega}^{(\text{out})}\right)^{-1}\left(\boldsymbol{b} - \boldsymbol{B}\boldsymbol{q}^{n+1(\text{in})}\right). \tag{25}$$

In the present paper, the following boundary conditions are used: a free boundary condition and an absorption condition. The following equation is used for the free boundary:

$$\boldsymbol{\sigma}\boldsymbol{n} = 0, \tag{26}$$

where $\boldsymbol{n}$ is the outward normal vector on the boundary, and σ is the Cauchy stress tensor. The right-hand side of Eq. (3) is the density of external forces on the boundary (it is zero for the case of a free boundary). The following equation is used as the absorption condition:

$$\boldsymbol{B} = \boldsymbol{\Omega}^{(*)}, \quad \boldsymbol{b} = \boldsymbol{0}, \tag{27}$$

where the matrix $\boldsymbol{\Omega}^{(*)}$ consists of the columns of the matrix of eigenvalues $\boldsymbol{\Lambda}$ corresponding to the outgoing characteristics.

5. NUMERICAL SIMULATION RESULTS

Seismic wave propagation was simulated for models with gas-saturated rocks in a layered ground for the three-dimensional case. The basic model had nine geological layers: water, silt, three layers of moisture-saturated sand, three layers of clay, and an oil-containing layer. A schematic diagram of the basic model is shown in Fig. 1. The numbers on the left, $0, 200, 350, \ldots, 1400$, indicate the depths of the geological layers. The upper boundary of the water layer and the lower boundary of the oil-containing layer were smooth, and the other boundaries were curvilinear. The numbers on the right, $150, 250, \ldots, 1170$, show maximum values of the lower curvilinear boundaries of the geological layers. The numbers on the top show the length and width of the model, which are equal to 2000 m.

As a rule, gas pockets are formed in pores of a sand layer. With time, they begin to spread in all directions due to high pressure inside the pockets [4]. Figure 2 presents a schematic diagram of propagation of gas-saturated rocks in a layered soil. The rectangle at the bottom is a gas pocket formed in the sand layer. The arrows show the direction of gas propagation. Figure 2 is also a schematic of the location of a transmitter-receiver system (a signal transmitter is denoted by the inverted triangle, and signal receivers are denoted by the triangles on the sides of the transmitter). A Ricker pulse with a central frequency of 30 Hz was used as the signal transmitter located at the center of the calculation domain on the water layer surface. 100 signal receivers were installed at the center of the calculation domain on the water layer surface with a spacing of 10 m. A free boundary condition [19] was set on the upper boundary of the calculation domain, with non-reflecting boundary conditions on the lateral and lower boundaries.

The parameters of the geological layers were as follows: the water density was 1000 kg/m^3, and the longitudinal wave speed in water was 1500 m/s. The silt density was 1600 kg/m^3, and the speeds of

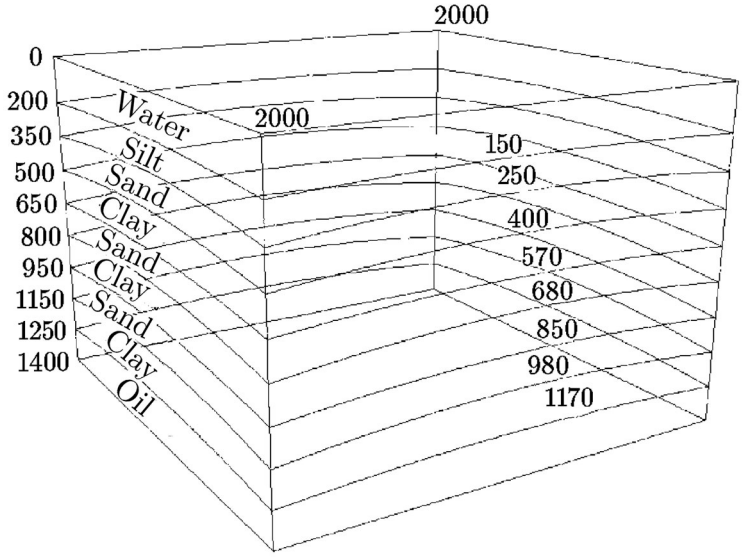

Fig. 1. Schematic diagram of the 2000 × 2000 m model.

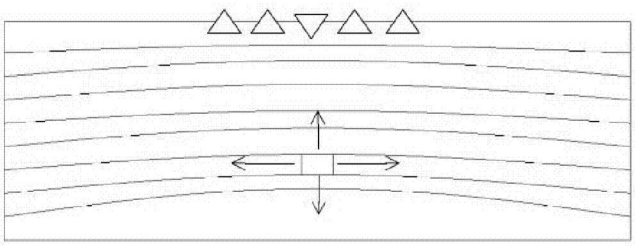

Fig. 2. Schematic diagram of gas propagation through a layered soil and location of a transmitter-receiver system.

longitudinal and transverse waves in the silt layer were 1600 m/s and 1131 m/s, respectively. The density of moisture-saturated sand was 1200 kg/m^3, and the velocities of longitudinal and transverse waves in the sand layer were 1600 m/s and 1131 m/s, respectively. The clay density was 2500 kg/m^3, and the speeds of longitudinal and transverse waves in the clay layer were 2000 m/s and 1414 m/s, respectively. The density of the oil-containing layer was 850 kg/m^3, and the speeds of longitudinal and transverse waves in the oil layer were 1400 m/s and 1000 m/s, respectively. The gas density was 900 kg/m^3, and the speeds of longitudinal and transverse waves in the gas pocket were 1000 m/s and 707 m/s, respectively. All layers of the basic model in Fig. 1, except for the upper water layer, had an average width of 150 m. The average width of the water layer was 200 m. The integration domain area was 4×10^6 m^2.

Figure 3 shows the models for the first, second, third, and fourth years of calculations. The height of all gas pockets was 150 m, the length and width was 200 m in the second year of calculations (Fig. 3b); 400 m and 200 m in the third year of calculations (Fig. 3c); and 600 m, 400 m, and 200 m in the fourth year of calculations (Fig. 3d).

In the calculations, the spacing in the x, y, and z axes in all models was 5 m. The time step was 10^{-4} s. A total of 20,000 time steps were made. The calculations for the four models were made using a shock-capturing method, with appropriate values of the density and speeds of longitudinal and transverse waves set for each point of the calculation domain. All calculations were made using the third order accurate Rusanov scheme [16]. The calculation time of the three-dimensional model on a stationary 4-core computer was 12 hours, and for the two-dimensional model it was 4 hours.

Figure 4 presents wave patterns of seismic responses.

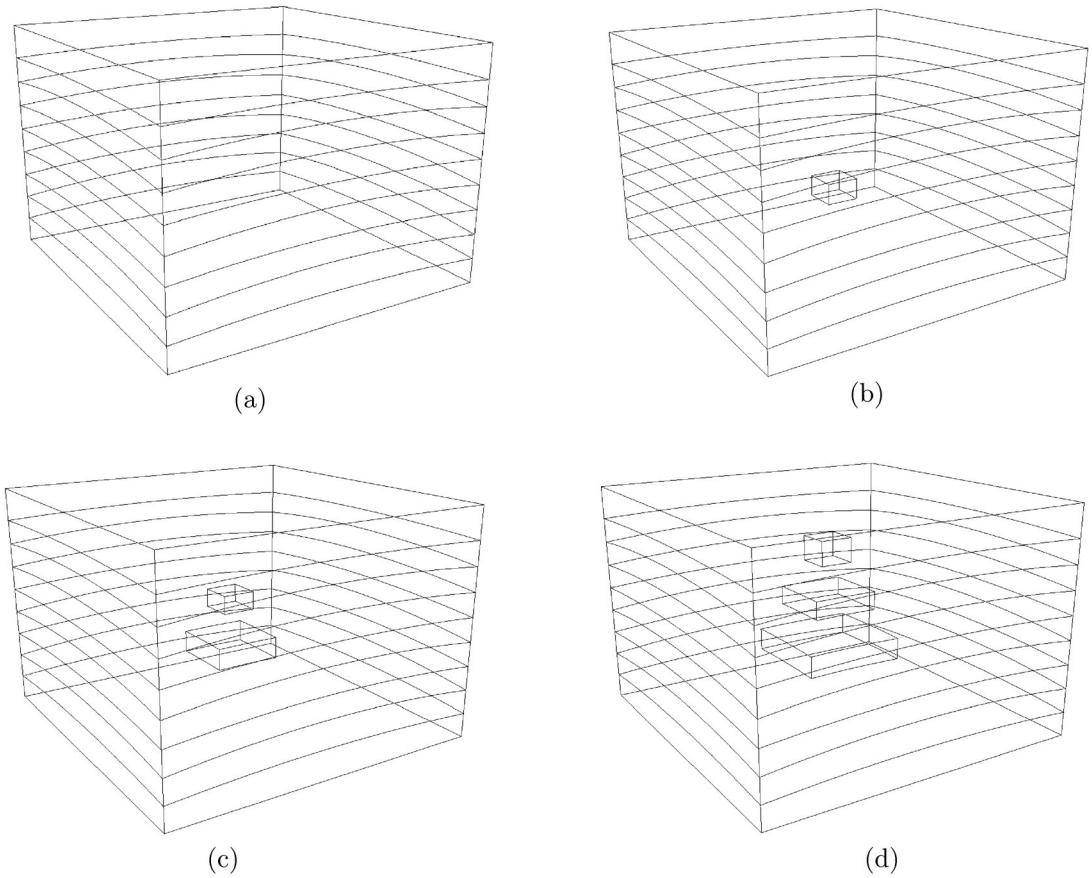

Fig. 3. Schematic diagrams of the models. (a) Model for the first year of calculations, no gas pockets; (b) model for the second year of calculations, one gas pocket; (c) model for the third year of calculations, two gas pockets; (d) model for the fourth year of calculations, three gas pockets.

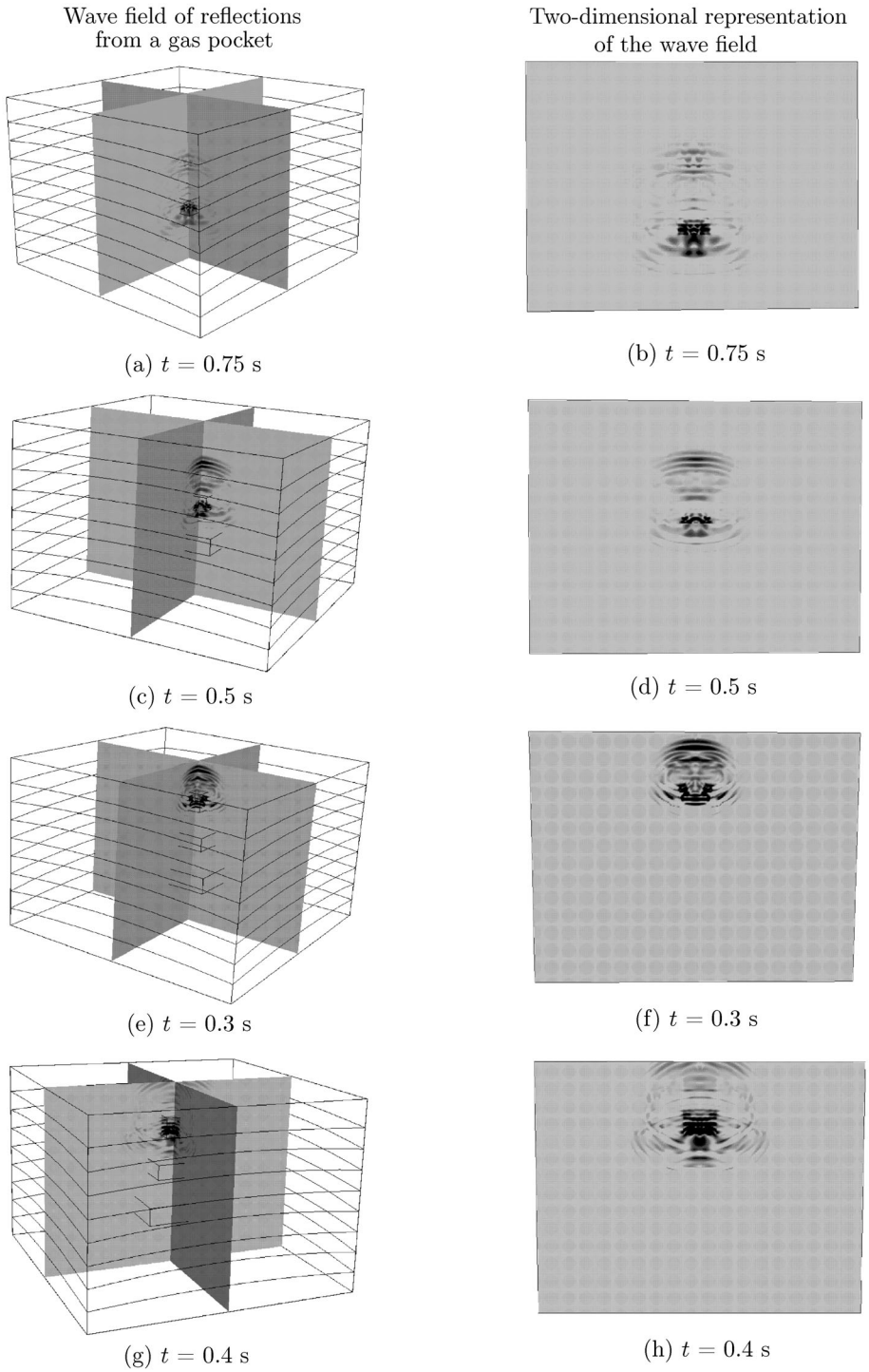

Fig. 4. Wave patterns of seismic responses of gas pockets for the second year of calculations (a, b), third year of calculations (c, d), and fourth year of calculations (e, f, g, h) for several times.

Figure 4 (left) shows the differences between the wave patterns for the second, third, and fourth years of calculations and the first year when there are no gas pockets, for obtaining wave responses directly from the gas pockets. Figure 4 (right) shows enlarged sections of two-dimensional wave patterns for the wave fields in the left part of Fig. 4. In the wave patterns, the gray color shades show the normal velocity components in the geological media from 0 m/s (no lines) to 5.5 m/s (black lines). One can

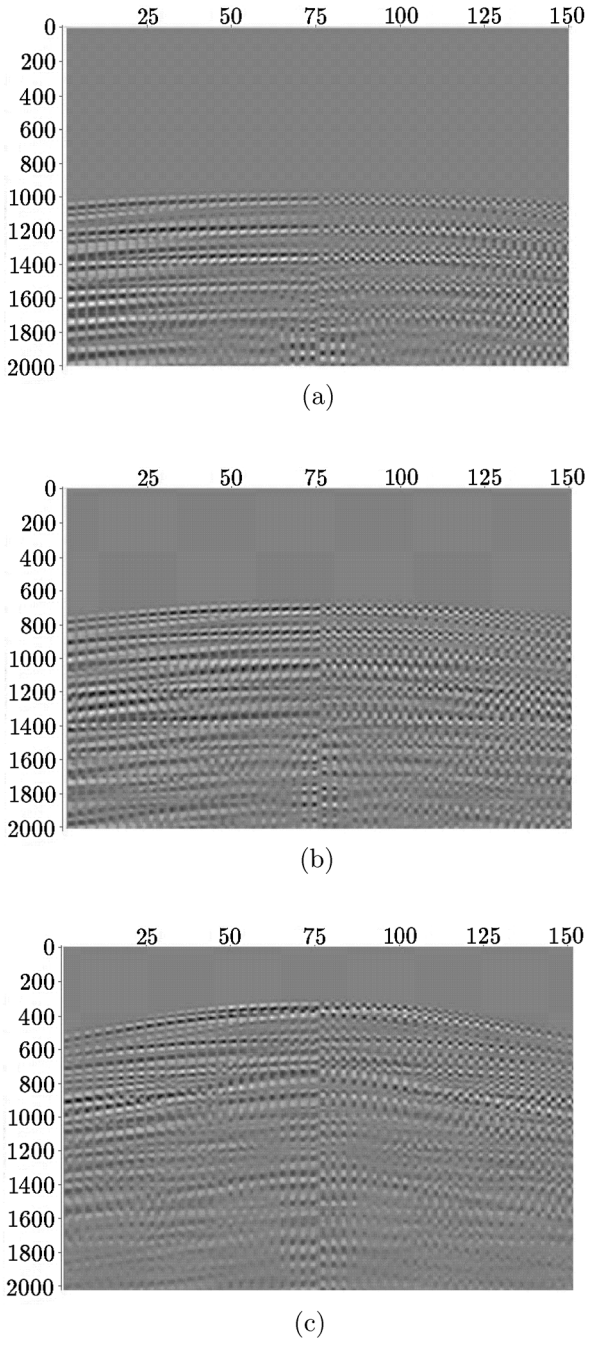

Fig. 5. Seismograms of wave responses for the second (a), third (b), and fourth (c) years of calculations. Normal velocity components (gray color shades), seismic traces (x axis), and signal arrival times in ms (y axis).

see in Figs. 4c and 4d that the gas pockets approach the water surface, which may cause, in the near future, gas emission into the atmosphere. Appropriate measures are needed to avoid further catastrophic consequences.

An important result is obtaining a so-called "gas pipe" [20]: gas migration channels extending to large depths (see Figs. 4a–4h). Such gas pipes are always visible on seismograms in geological surveys, but it is much more difficult to obtain them by simulation.

Figure 5 shows seismograms of wave responses of the gas pockets for the second, third, and fourth years of calculations. The seismograms in Fig. 5 are the differences between these seismograms and those for the first year of calculations to obtain seismic signals only from the gas pockets. In Fig. 5 the

gray color shades show the normal velocity components, where the x axis shows seismic traces 1–150, and the y axis shows signal arrival times 0–2000 ms. The seismograms in Fig. 5 show the dynamics of signal increase with time from the second to fourth year of calculations. On the fourth year of calculations (Fig. 5c), the gas approaches the water surface and may cause gas emission into the atmosphere. This result is in agreement with the gas approach to the water surface shown in the wave patterns for the fourth year of calculations (see Figs. 4e–4h).

6. CONCLUSIONS

In this paper, the results of numerical simulations of seismic wave propagation in models with gas-saturated rocks in a layered soil in the three-dimensional case have been presented.

Equations for the propagation of elastic waves in a linear elastic medium have been formulated. A grid-characteristic method and the boundary conditions used in all model calculations have been described. A basic model of the layered medium used in all calculations has been characterized. All characteristics of the geological layers of the model (density, geometric dimensions, longitudinal and transverse wave velocities) were given.

Wave patterns of seismic responses of the gas pockets were analyzed. It has been shown that on the fourth year of calculations the gas-saturated rocks approach the water surface, which may cause, in the near future, emission into the atmosphere.

Seismograms of responses for the models of the second, third, and fourth years of calculations were presented. Their analysis (as well as the analysis of wave patterns) has shown that the gas can approach the water surface on the fourth year of calculations.

The results of the simulations of seismic wave propagation in the three-dimensional models with gas-saturated rocks on curvilinear grids using the shock-capturing method showed good agreement with results of real geological surveys in a similar problem statement. The wave patterns and seismograms for the three-dimensional models are in good agreement with the results of similar studies for two-dimensional models obtained by the authors earlier [9, 10]. This is very important, since the calculations can be greatly simplified by replacing the three-dimensional models with the two-dimensional ones in similar problem statements.

FUNDING

This work was supported by the Ministry of Education and Science of the Russian Federation (project no. 2.9901.2017/8.9).

REFERENCES

1. Mironyuk, S.G., Marine Engineering Studies and Danger Assessment of Subaquatic Geological Processes, *Inzhener. Izysk.*, 2014, vol. 4, pp. 60–64.
2. Aleksandrov, B.L., *Anomal'no vysokie plastovye davleniya v neftegazonosnykh basseinakh* (Anomalously High Formation Pressures in Oil and Gas Deposits), Moscow: Nedra, 1987.
3. Hovland, M. and Judd, A.G., *Seabed Pockmarks and Seepages. Impact on Geology, Biology and the Marine Environment*, London: Graham and Trotman, 1988.
4. Judd, A. and Hovland, M., *Seabed Fluid Flow: The Impact on Geology, Biology and the Marine Environment*, Cambridge, 2007.
5. Syvorotkin, V.L., Deep Degassing of the Earth and Geoecological Problems in Frontier Areas of Russia, *Almanac "Space and Time." Special Issue "Space, Time, and Boundaries"*, 2013, vol. 3, no. 1, pp. 1–19.
6. Bogoyavlensky, V.I., Kerimov, V.Yu., Olkhovskaya, O.O., and Mustaev, R.N., Improving the Efficiency and Safety of Prospecting, Exploration and Development of Oil and Gas Fields in the Sea of Okhotsk, *Territoriya Neftegas*, 2016, vol. 10, pp. 24–32.
7. Boogaard, M. and Hoetz, G., *Seismic characterisation of shallow gas in the Netherlands* Abstract FORCE Seminar, Stavanger, 2015.
8. Rokos, S.I., Gas Saturated Deposits of the Upper Section of the Barents-Kara Shelf, Cand. Sci. (Geogr.) Dissertation, Murmansk, 2009.
9. Stognii, P.V. and Khokhlov, N.I., 2D Seismic Prospecting of Gas Pockets, *Smart Innovations, Systems Technol.*, 2019, vol. 133, pp. 156–166.

10. Stognii, P., Breus, A., and Khokhlov, N., Numerical Modelling of Seismic Waves Spread with the Presence of Gas Layers in the Arctic Region, *Proc. 20th Conf. on Oil and Gas Geological Exploration and Development "Geomodel 2018,"* 2018, pp. 465–469.
11. Stognii, P.V., Petrov, D.I., Khokhlov, N.I., and Petrov, I.B., Simulation of Seismic Processes in Geological Exploration of Arctic Shelf, *Russ. J. Numer. An. Math. Model.*, 2017, vol. 32, no. 6, pp. 381–392.
12. Novatsky, V., *Teoriya uprugosti* (Theory of Elasticity), Moscow: Mir, 1975.
13. Magomedov, K.M. and Kholodov, A.S., *Grid-Characteristic Numerical Methods*, M.: Nauka, 1988.
14. Khokhlov, N. and Stognii, P., Novel Approach to Modeling the Seismic Waves in the Areas with Complex Fractured Geological Structures, *Minerals*, 2020, vol. 10, no. 2, pp. 122; URL: https:doi.org/10.3390/min10020122.
15. Golubev, V.I., Petrov, I.B., and Khokhlov, N.I., Numerical Simulation of Seismic Activity by the Grid-Characteristic Method, *Comp. Math. Math. Phys.*, 2013, vol. 53, no. 10, pp. 1523–1533.
16. Kholodov, A.S. and Kholodov, Ya.A., Monotonicity Criteria for Difference Schemes Designed for Hyperbolic Equations, *Zh. Vych. Mat. Mat. Fiz.*, 2006, vol. 46, no. 9, pp. 1638–1667.
17. Ivanov, A.M. and Khokhlov, N.I., Parallel Implementation of the Grid-Characteristic Method in the Case of Explicit Contact Boundaries, *Comp. Res. Model.*, 2018, vol. 10, no. 5, pp. 667–678.
18. Golubev, V.I., Petrov, I.B., Khokhlov, N.I., and Shul'ts, K.I., Numerical Computation of Wave Propagation in Fractured Media by Applying the Grid-Characteristic Method on Hexahedral Meshes, *Zh. Vych. Mat. Mat. Fiz.*, 2015, vol. 55, no. 3, pp. 512–522.
19. Favorskaya, A., Golubev, V., and Khokhlov, N., Two Approaches to the Calculation of Air Subdomains: Theoretical Estimation and Practical Results, *Procedia Comp. Sci.*, 2018, vol. 126, pp. 1082–1090.
20. Bogoyavlensky, V.I., The Threat of Catastrophic Gas Emissions from the Arctic Cryolithozone. Craters of Yamal and Taimyr, *Burenie Neft'*, 2014, vol. 9, pp. 13–18.